Editors' Suggestion

Heat transport in nonlinear lattices free from the umklapp process

Kazuyuki Yoshimura,[1] Yusuke Doi,[2] and Tomoya Kitamura[3]
[1]*Faculty of Engineering, Tottori University, 4-101 Koyama-Minami, Tottori 680-8552, Japan*
[2]*Division of Mechanical Engineering, Graduate School of Engineering, Osaka University, 2-1 Yamadaoka, Suita, Osaka 565-0871, Japan*
[3]*Department of Engineering, Graduate School of Sustainability Science, Tottori University*
4-101 Koyama-Minami, Tottori 680-8552, Japan

(Received 5 August 2021; accepted 16 December 2021; published 28 February 2022)

We construct one-dimensional nonlinear lattices having the special property such that the umklapp process vanishes and only the normal processes are included in the potential functions. These lattices have long-range quartic nonlinear and nearest-neighbor harmonic interactions with/without harmonic onsite potential. We study heat transport in two cases of the lattices with and without harmonic onsite potential by nonequilibrium molecular dynamics simulation. It is shown that the ballistic heat transport occurs in both cases, i.e., the scaling law $\kappa \propto N$ holds between the thermal conductivity κ and the lattice size N. This result directly validates Peierls's hypothesis that only the umklapp processes can cause the thermal resistance while the normal ones do not.

DOI: 10.1103/PhysRevE.105.024140

I. INTRODUCTION

Heat transport is ubiquitous in nature. In macroscopic-scale materials, it is well described by the Fourier's law $J = -\kappa \nabla T$, where J and ∇T are the heat flux and the temperature gradient, respectively, and κ is a constant called the thermal conductivity, whose value is determined by the material. Consider a one-dimensional shaped material with length L which is kept with different temperatures at the both ends. The Fourier's law implies that the heat flux J is attenuated as $J \propto L^{-1}$ with increasing L, under a given temperature difference. This attenuation indicates the existence of thermal resistance. In microscopic scale, the value of κ depends on both the material and its length [1], but the heat flux is still attenuated as the length increases, i.e., the thermal resistance still emerges. It has been a long-standing unsolved problem to clarify the origin of thermal resistance based on the dynamics of atoms.

A simple microscopic model for solids is one-dimensional lattice, and it has been used for studying heat transport via atomic vibrations [2,3]. Nonlinearity of the lattice, which is necessary for the phonon interactions, is essential to explain the emergence of thermal resistance. There are two types of the phonon interaction processes, which are called the *normal* and the *umklapp* processes. Peierls posed the hypothesis that only the umklapp processes can cause the thermal resistance while the normal ones do not [4,5], and this hypothesis has been widely believed so far. However, at least in the classical physics regime, the hypothesis does not have a firm theoretical basis. To the best of our knowledge, only the existing basis is that in a lattice with periodic boundary conditions the harmonic part of its total heat flux is conserved if there is no umklapp process, provided that the lattice has *no dispersion* [5–7]. The assumption of no dispersion is never satisfied in one-dimensional lattices, and this is not a satisfactory basis for the hypothesis.

The above hypothesis has not yet been verified even by numerical simulations. The crucial reason is a lack of a nonlinear lattice model that is free from the umklapp process. In the present paper, we construct a class of nonlinear lattices without the umklapp process, which we call the *umklapp-free lattices* (UFLs). The UFLs have long-range quartic nonlinear and nearest-neighbor harmonic interactions with/without harmonic onsite potential. They closely relate with the *pairwise interaction symmetric lattice* (PISL) [8,9], which is a special lattice model recently constructed and having a hidden symmetry in its potential function to enhance the mobility of a localized mode called the *discrete breather* [10–13].

The UFL enables one to directly verify Peierls's hypothesis. We numerically study heat transport in two types of UFLs, which are with and without harmonic onsite potential, and show that the ballistic heat transport occurs in both of the UFLs, i.e., $\kappa \propto N$ holds between the thermal conductivity κ and the lattice size N. Our results justify Peierls's hypothesis at least in the present lattice models.

We mention known results about heat transport in the PISL, as it is a model closely related to the UFL. A near ballistic transport, $\kappa \propto N^{\alpha}$ with $\alpha \simeq 1$, has been reported in some works [14–17], whereas a different value $\alpha \simeq 0.71$ in Ref. [18]. It is still unclear whether the PISL exhibits the ballistic transport or nonballistic but anomalous one. However, at least, the PISL seems to have α significantly larger than nonlinear lattices which are known to exhibit anomalous heat transport such as the FPUT-α or β lattices ($0.3 \lesssim \alpha \lesssim 0.4$).

We emphasize a significance of our model from the point of view of future studies. The UFL is expected to be a good starting point to study the mechanism of emerging of thermal resistance. It is possible to gradually introduce the umklapp processes into the UFL by perturbing its potential functions. Therefore, the mechanism may be clarified by numerically observing what kind of elementary process is occurring in the

perturbed UFL, i.e., by identifying the scatterer and scattering process of phonons.

This paper is organized as follows. In Sec. II, we describe the UFL model. In Sec. III, we describe details of our numerical simulation of heat transport in the UFL. In Sec. IV, we show numerical results of the simulation. Finally, conclusions are drawn in Sec. V.

II. UMKLAPP-FREE LATTICE MODEL

The model we constructed is a class of infinite lattices with long-range nonlinear interactions which is described by the Hamiltonian

$$H = \sum_{n=-\infty}^{\infty} \frac{1}{2} p_n^2 + \sum_{n=-\infty}^{\infty} \left[\frac{\mu_0}{2} q_n^2 + \frac{\mu_1}{2} (q_{n+1} - q_n)^2 \right] + \beta \sum_{n=-\infty}^{\infty} \sum_{r=1}^{\infty} \frac{1}{4r^2} \{q_{n+r} - (-1)^r q_n\}^4. \tag{1}$$

This model corresponds to a one-dimensional chain of unit-mass particles, where nth particle has its position $x_n = an + q_n$ given by the lattice spacing constant a and the relative displacement q_n. In Eq. (1), p_n is the momentum of nth particle, μ_0 and μ_1 are coefficients of the harmonic onsite and interaction potentials, and $\beta > 0$ is the nonlinearity strength. Arbitrary nonnegative values are possible for μ_0 and μ_1. The coupling strength between the rth neighboring particles is proportional to $1/r^2$. We call this lattice the UFL. Note that the UFL should be regarded as only a mathematically idealized model since the nonlinear interaction term in Eq. (1) is physically unnatural due to the factor $(-1)^r$.

The equations of motion derived from the Hamiltonian Eq. (1) are given by

$$\ddot{q}_n = -\mu_0 q_n + \mu_1 (q_{n+1} - 2q_n + q_{n-1}) + \beta \sum_{r=1}^{\infty} \frac{1}{r^2} [\{(-1)^r q_{n+r} - q_n\}^3 - \{q_n - (-1)^r q_{n-r}\}^3], \tag{2}$$

where $n \in \mathbb{Z}$. Note that the total momentum $\sum_{n=-\infty}^{\infty} p_n$ is not conserved by Eq. (2) regardless of the value of μ_0, as shown in Appendix A.

Define the normal mode coordinates $U(k)$ via the discrete Fourier transformation

$$U(k) = \frac{1}{\sqrt{2\pi}} \sum_{n=-\infty}^{\infty} q_n e^{-ikn}, \tag{3}$$

where we restrict the range of wave number k to the first Brillouin zone, i.e., $k \in \mathbb{T} \equiv (-\pi, \pi]$. If we rewrite Eq. (2) in terms of $U(k)$, then we can obtain the equation

$$\ddot{U}(k) + \nu_k^2 U(k) = \frac{4\beta}{\pi} \int_{\mathbb{T}^3} dk_1 dk_2 dk_3 \phi_0(k_1, k_2, k_3, k) \times U(k_1) U(k_2) U(k_3) \delta(k_1 + k_2 + k_3 - k), \tag{4}$$

where $U(k)$ depends on time t, ϕ_0 is a time-independent function of (k_1, k_2, k_3, k), δ is Dirac delta function, and ν_k^2 is given by

$$\nu_k^2 = \mu_0 + 4\mu_1 \sin^2(k/2). \tag{5}$$

Details of the derivation of Eq. (4) are described in Appendix B.

Ordinary one-dimensional lattices with quartic potentials have the mode couplings specified by both $k_1 + k_2 + k_3 - k = 0$ and $\pm 2\pi$ (cf. Appendix B1). The former $k_1 + k_2 + k_3 - k = 0$ is called the normal process while the latter $k_1 + k_2 + k_3 - k = \pm 2\pi$ the umklapp process. Equation (4) shows that four normal modes are coupled only when their wave numbers satisfy the condition $k_1 + k_2 + k_3 - k = 0$ while the couplings of $\pm 2\pi$ are not allowed. This mode coupling rule is a peculiarity of the UFL, and it indicates the nonexistence of the umklapp process. As mentioned in Sec. I, the UFL closely relates with the PISL. Their relation is described in Appendix C.

III. SIMULATION SETUP

To study the heat transport by nonequilibrium molecular dynamics simulation, we introduce an approximate version of the UFL which has truncated long-range interactions up to length M, which we call the *truncated UFL*. This lattice is not exactly free from the umklapp processes: the mode coupling terms specified by $k_1 + k_2 + k_3 - k = \pm 2\pi$ appear in its equation of motion in the normal mode coordinates $U(k)$. Those umklapp terms become smaller and vanish as $M \to +\infty$. Thus, the truncated UFL satisfies the condition of nonexistence of the umklapp process in good approximation when M is large enough.

In numerical simulations, we use a finite-size truncated UFL equipped with stochastic Langevin thermostats in its both ends. The equations of motion of our simulation model are given as follows:

$$\ddot{q}_n = \lambda(q_{n+1} - 2q_n + q_{n-1}) - \gamma \dot{q}_n + \zeta_n(t) \tag{6}$$

for $n \in I_H \cup I_L$ and

$$\ddot{q}_n = -\mu_0 q_n + \mu_1 (q_{n+1} - 2q_n + q_{n-1}) + \beta \sum_{r=1}^{M} \frac{1}{r^2} [\{(-1)^r q_{n+r} - q_n\}^3 - \{q_n - (-1)^r q_{n-r}\}^3] \tag{7}$$

for $n \in I$, where $I_H = \{1, 2, \ldots, n_0\}$ and $I_L = \{N + n_0 + 1, \ldots, N + 2n_0\}$ are the sets of indices of particles equipped with high and low temperature thermostats, respectively, and $I = \{n_0 + 1, \ldots, n_0 + N\}$ is the set of indices for the truncated UFL. The constant λ can be different from μ_1, but we assume $\lambda = \mu_1$ in the present simulation for simplicity. The range of nonlinear interactions is truncated up to M in the model. In addition, the sum in Eq. (7) is taken only for the terms $\{(-1)^r q_{n+r} - q_n\}^3$ satisfying $n + r \leqslant n_0 + N$ and the terms $\{q_n - (-1)^r q_{n-r}\}^3$ satisfying $n - r \geqslant n_0 + 1$. This implies that the nearest-neighbor harmonic coupling is assumed between n_0 and $n_0 + 1$ particles and between $n_0 + N$ and $n_0 + N + 1$ particles, which are connections between the truncated UFL and the heat baths. As for the boundary

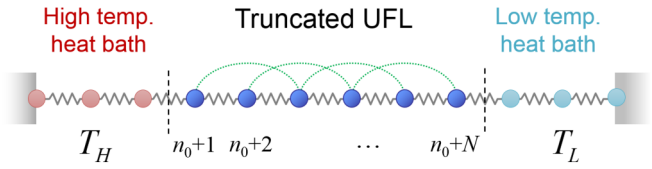

FIG. 1. Illustration of simulation model. Green dotted line represents the long-range interaction, where $M = 2$ case is illustrated.

conditions, we assume $q_0 = q_{N+2n_0+1} = 0$. Figure 1 illustrates the simulation model.

In Eq. (6), $-\gamma\dot{q}_n + \zeta_n(t)$ represents the Langevin thermostat, where $\gamma > 0$ is a constant and $\zeta_n(t)$ is the white Gaussian noise having the properties

$$\langle \zeta_n(t) \rangle = 0, \tag{8}$$

$$\langle \zeta_n(t)\zeta_m(s) \rangle = 2\gamma T \delta_{n,m}\delta(t-s), \tag{9}$$

where $\langle\cdot\rangle$ denotes the averaging over realizations of $\zeta_n(t)$, $\delta_{n,m}$ is Kronecker delta, and δ is Dirac delta function. The parameter T represents the thermostat temperature, which is set as $T = T_H$ and T_L for the high and low temperature sides, respectively.

The heat flux can be measured via a simple expression at the boundaries of the truncated UFL, i.e., $n = n_0 + 1$ and $n_0 + N$ particles. Each of these two particles is coupled with its nearest-neighbor thermostated particle via harmonic interaction force only. Noting this fact, we obtain the expression for the heat flux J_1, which is the energy transported from n_0th particle to $(n_0 + 1)$th one per unit time, as follows:

$$J_1 = -\langle \dot{q}_{n_0+1} \cdot \mu_1 (q_{n_0+1} - q_{n_0}) \rangle_\tau, \tag{10}$$

where $\langle\cdot\rangle_\tau$ represents averaging over a long time τ, i.e., $\langle X \rangle_\tau = \tau^{-1} \int_0^\tau X(t)dt$ for an arbitrary quantity $X(t)$. Similarly, we can obtain the heat flux J_2 at $(n_0 + N)$th particle as follows:

$$J_2 = -\langle \dot{q}_{n_0+N} \cdot \mu_1 (q_{n_0+N+1} - q_{n_0+N}) \rangle_\tau. \tag{11}$$

If we measure the heat flux at an inner particle of the truncated UFL with $n \in \{n_0 + 2, \ldots, n_0 + N - 1\}$, then we will have a more complex expression of heat flux due to the long-range interactions. So, we chose the two boundary particles. In the simulation, we compute the heat flux J by the average of J_1 and J_2, i.e.,

$$J = \tfrac{1}{2}(J_1 + J_2). \tag{12}$$

The thermal conductivity κ is defined by

$$\kappa = \frac{J}{(T_H - T_L)/N}. \tag{13}$$

We will focus on the N-dependence of κ. It is well known that one-dimensional lattices exhibit the power law $\kappa \propto N^\alpha$ with $0 \leqslant \alpha \leqslant 1$ [7]. The heat transport is called *normal* when $\alpha = 0$ while it is called *anomalous* when $\alpha > 0$. In particular, it is called the *ballistic* heat transport when $\alpha = 1$, and this implies the state of vanishing thermal resistance.

We introduce spectral energy flux to study the heat transport process in detail. If we neglect the nonlinear forces and only consider the harmonic one in Eq. (2), then we can define the harmonic part of the total heat flux as follows:

$$J_{H,\mathrm{tot}} = -\frac{\mu_1}{2} \sum_{n=n_0+1}^{n_0+N-1} (\dot{q}_{n+1} + \dot{q}_n)(q_{n+1} - q_n). \tag{14}$$

Let $u_k \in \mathbb{C}$, $k = -N/2 + 1, \ldots, N/2$ be the mode amplitudes defined by the transformation

$$q_{n_0+n} = \frac{1}{\sqrt{N}} \sum_{k=-N/2+1}^{N/2} u_k \exp\left[-i\frac{2\pi k}{N} n\right], \quad n = 1, 2, \ldots, N, \tag{15}$$

where $u_{-k} = \bar{u}_k$ holds since $q_{n_0+n} \in \mathbb{R}$. $\bar{u}_k$ stands for the complex conjugate of u_k. In terms of u_k, we can decompose $J_{H,\mathrm{tot}}$ into the form $J_{H,\mathrm{tot}} = \sum_{k=1}^{N/2-1} J_H(k)$ with

$$J_H(k) = 2\omega_k v_k \,\mathrm{Im}[\dot{u}_k \bar{u}_k], \quad k = 0, 1, \ldots, N/2, \tag{16}$$

where ω_k and v_k are defined by $\omega_k = 2\sqrt{\mu_1}\,|\sin(\pi k/N)|$ and $v_k = \sqrt{\mu_1}\,\mathrm{sgn}(k)\cos(\pi k/N)$. This quantity $J_H(k)$ is the harmonic part of the net energy flux carried by two modes with wave numbers $\pm k$. The derivation of Eq. (16) is described in Appendix D.

IV. SIMULATION RESULTS

We numerically solved Eqs. (6) and (7) to compute the thermal conductivity κ for different lattice sizes N, by using the Verlet scheme with time step $\Delta t = 0.05$. Computation of the long-range nonlinear interaction forces in Eq. (7) is time-consuming for large values of M. To overcome this difficulty, we utilized GPU (NVIDIA GeForce RTX3080) for high-speed computation. The parameter values used in the simulation are $\lambda = 1$, $\gamma = 0.2$, $T_H = 1.2$, $T_L = 0.8$, and $n_0 = 10$.

Figures 2(a) and 2(b) show the logarithmic plots of κ as a function of N for $\mu_0 = 0$ and $\mu_0 = 1$ cases, i.e., the lattices without and with harmonic onsite potential, respectively. The weakly nonlinear case of $\mu_1 = 1$ and $\beta = 0.1$ is assumed. The numerical results are shown for different values of the coupling length M from $M = 1$ to 512.

In the simulations, we monitored the heat flux J given by Eq. (12) as a function of τ, which tends to converge to a constant as the averaging period τ increases. We used the convergence of $J(\tau)$ as a criterion for the system to have reached a steady state. In addition, we also monitored convergence of the spatial temperature profile (cf. Fig. 3).

In Fig. 2(a), the scaling of κ with respect to N precisely coincides with the ballistic one $\kappa \propto N$ over the whole range of simulation, i.e., up to $N = 2^{20}$, in the case of $M = 512$. For smaller values of M, the scaling is close to $\kappa \propto N$ as N increases up to a certain value N_c, but it deviates from $\kappa \propto N$ as N further increases. The values of N_c are approximately found as $N_c \simeq 2^{19}$, 2^{14}, and 2^{11} for $M = 256$, 64, and 16, respectively. N_c decreases as M decreases. In Fig. 2(b), qualitatively the same behavior of κ is observed. The ballistic transport is clearly observed for $M = 512$ also in Fig. 2(b).

We are interested in the asymptotic scaling of κ in the limit $N \to +\infty$, although numerical results are available only for

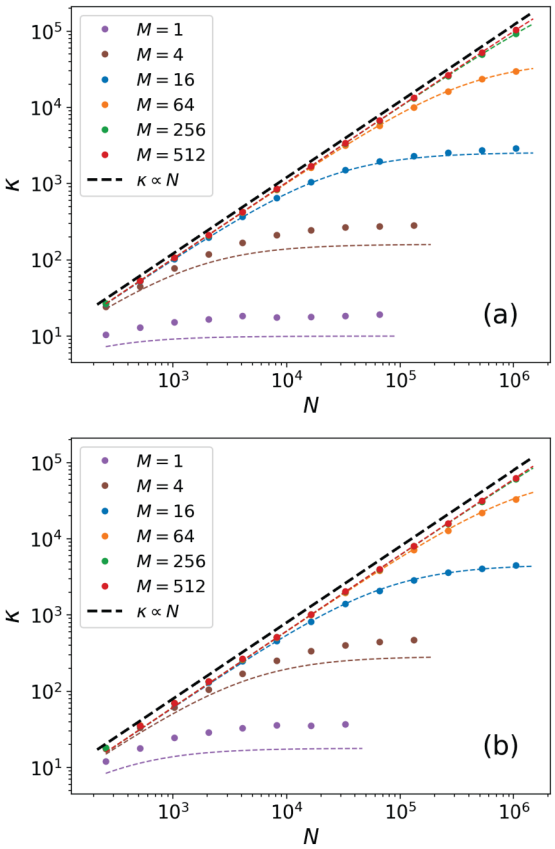

FIG. 2. Thermal conductivity κ vs lattice size N for truncated UFL ($\mu_1 = 1$, $\beta = 0.1$) (a) without onsite potential ($\mu_0 = 0$) and (b) with onsite potential ($\mu_0 = 1$). Results are shown by filled circles for different values of M. Temperatures are $T_H = 1.2$ and $T_L = 0.8$. Black dashed line represents the ballistic power law $\kappa \propto N$. Colored dashed lines are the fitting curves by experimental formula Eq. (17).

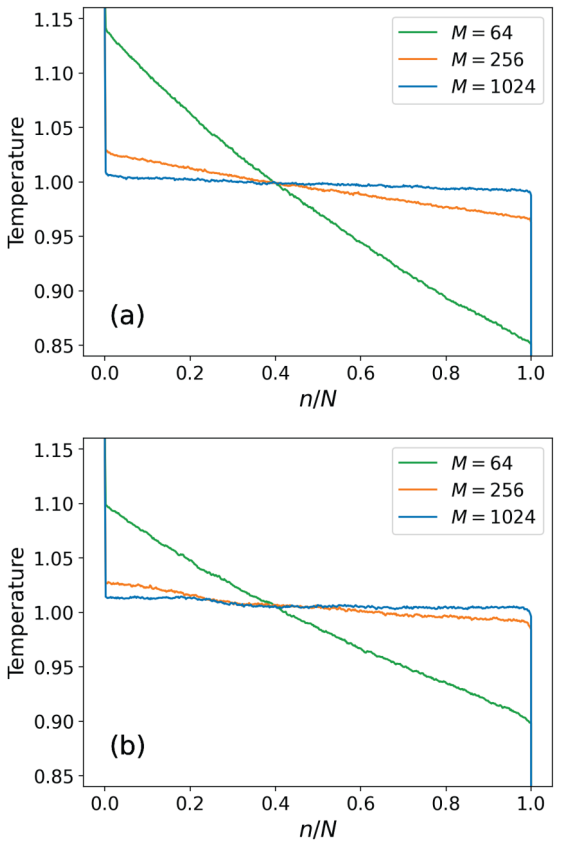

FIG. 3. Temperature profile plotted vs n/N for the truncated UFL ($\mu_1 = 1$, $\beta = 0.1$) (a) without onsite potential ($\mu_0 = 0$) and (b) with onsite potential ($\mu_0 = 1$). Profiles are shown for $M = 64$, 256, and 1024. Parameters are $N = 2^{20}$, $T_H = 1.2$, and $T_L = 0.8$.

finite N values. An experimental formula is useful to infer the asymptotic scaling, and we have found it in the form

$$\kappa = \frac{aN}{1 + bN/M^2}, \tag{17}$$

where a and b are the fitting parameters and their values are obtained as $a = 0.1032$, $b = 0.009904$ for $\mu_0 = 0$ and $a = 0.06314$, $b = 0.004169$ for $\mu_0 = 1$, respectively. In Figs. 2(a) and 2(b), the curves of Eq. (17) with these values of (a, b) are also shown. A good agreement between Eq. (17) and the numerical results is confirmed in each figure, except for the small M cases of $M = 1$ and 4. This agreement suggests that it is a reasonable experimental formula at least for values of M not too small. Once we accept Eq. (17), we can infer the behavior of κ in the limit $N \to +\infty$. Equation (17) indicates that the asymptotic scaling $\kappa \propto N$ holds if we take the limit $N \to +\infty$ keeping the ratio M/N as a constant.

As shown in Figs. 2(a) and 2(b), the truncated UFLs with $M = 512$, where the nonexistence of the umklapp process holds in good approximation, exhibit the ballistic heat transport regardless of harmonic onsite potential. In contrast, in the cases of nonnegligible umklapp process, i.e., smaller M cases, the ballistic heat transport breaks down for $N > N_c$. Based on these numerical observations and the inference via Eq. (17), it may be concluded that the thermal resistance is never caused by the normal processes but only by the umklapp ones. That is, we have validated Peierls's hypothesis. We remark that it is not clear here whether all the umklapp processes are resistive or only some of them are so.

One might expect the possibility that the ballistic transport in the UFL is caused simply by instantaneous energy transport over long distances via the long-range interaction forces. This issue has been studied for some nonlinear lattices with the long-range coupling coefficient $1/r^c$ [19]. It has been shown that for $c > 1$ such long-distance transport is nondominant. This result is suggestive that the ballistic transport in UFL is being caused by the lack of umklapp process.

The ballistic transport observed in the UFL is somewhat surprising from the fact that the total momentum is not conserved by Eq. (2). Table I summarizes known results for the type of heat transport and the total momentum conservation property in several one-dimensional nonlinear lattices. A common belief is that momentum nonconserving lattices belong to the class of normal heat transport, and this belief has been corroborated in various such lattices [20–26]. As Table I shows, all the momentum nonconserving lattices studied so far exhibit the normal heat transport, except for an example mentioned below. We emphasize that the UFL is a counterexample against this common belief.

TABLE I. Classification of nonlinear lattice models by the type of heat transport and the total momentum conservation property.

	Nonconserving	Conserving
Normal $\alpha = 0$	Ding-a-ling [20,21] Ding-dong [22] Frenkel-Kontrova [23] ϕ^4 chain [24,25] Toda+harmonic onsite [26]	Coupled rotators [27] Modified ding-a-ling [28]
Anomalous $0 < \alpha < 1$		FPUT-α [29] FPUT-β [30,31] Diatomic Toda [32]
Ballistic $\alpha = 1$	UFL	Toda [33]

In Table I, we listed only nonlinear lattices of the natural Hamiltonian type, i.e., $H = \sum p_n^2/2 + V(q_1, \ldots, q_N)$. Other than this type, the ballistic transport has been reported for the Izergin-Korepin discrete sine-Gordon model, which is an integrable and momentum nonconserving model [34]. We also mention that there is a momentum-conserving coupled map lattice which exhibits the normal transport [35]. This model was derived from a Hamiltonian system with periodic impulsive kicks.

The PISL is momentum nonconserving when it has a harmonic onsite potential, otherwise it is momentum conserving. Its heat transport property has been studied for the momentum conserving PISL in Refs. [14,15,17,18] while for both types of PISLs in Ref. [16]. Scaling laws close to the ballistic transport, i.e., $\kappa \propto N^\alpha$ with $\alpha \simeq 1$, are obtained in Refs. [14–17], whereas a different value $\alpha \simeq 0.71$ is reported in Ref. [18]. Reasons for this discrepancy in α are discussed in Ref. [17]. At this point, a definitive conclusion has not been settled in about the value of α, and it is unclear whether the PISLs exhibit the ballistic transport or nonballistic but anomalous one. So, we did not include the PISL in Table I.

Figures 3(a) and 3(b) show the spatial profile of temperature T as a function of n/N for $\mu_0 = 0$ and 1, respectively, where $N = 2^{20}$, n is the site number, and the local temperature T is defined by the time average of kinetic energy, i.e., $T = \langle p_n^2 \rangle_\tau$. The results are shown for $M = 64$, 256, and 1024. Apart from steep temperature variation in the regions close to the heat baths, the temperature gradient becomes smaller as M increases, and the flat profile is formed for $M = 1024$, in each figure. This flat profile is one of the characteristics of the ballistic heat transport.

The harmonic energy flux J_H is plotted against k/N for $\mu_0 = 0$ and 1 in Fig. 4 for different N, respectively, where $M = 512$ is fixed. The other parameter values are the same as in Fig. 2. This figure indicates that contribution of the nonlinearity in heat transport is substantial since the profiles of J_H are much different between the truncated UFLs and the harmonic lattices. This fact confirms that the ballistic transport observed in Fig. 2 is not due to a predominance of the linearity. The curves of $J_H(k/N)$ for different N values coincide with each other in both cases of $\mu_0 = 0$ and 1. The total amount of J_H over the interval $k/N \in [0, 0.5]$, which is defined by

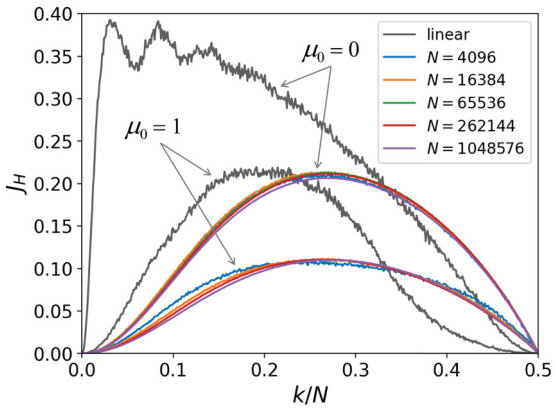

FIG. 4. Spectrum of harmonic energy flux J_H plotted vs k/N. Results are shown for truncated UFLs ($\mu_1 = 1$, $\beta = 0.1$) without onsite potential ($\mu_0 = 0$) and with onsite potential ($\mu_0 = 1$), where $M = 512$, $T_H = 1.2$, and $T_L = 0.8$. Results are shown for $N = 2^{12}$, 2^{14}, 2^{16}, 2^{18}, and 2^{20}. J_H for harmonic lattices ($\mu_1 = 1$, $\beta = 0$) with $\mu_0 = 0$ and 1 are shown by black line for comparison.

$\bar{J}_H = \int_0^{0.5} J_H(s)\, ds$ with $s = k/N$, is almost independent of N. This fact is consistent with the ballistic scaling $\kappa \propto N$. We note that $\bar{J}_H$ does not coincides with $J_{H,\mathrm{tot}}$: they relate with each other as $\bar{J}_H \simeq J_{H,\mathrm{tot}}/N$. Comparing the profiles of curves of $J_H(k/N)$ between $\mu_0 = 0$ and 1 cases, there is a significant difference. This fact suggests that in our simulation the heat transport state is in actual influenced by the onsite potential, although only similar results are observed in Figs. 2 and 3 between $\mu_0 = 0$ and 1 cases.

Figure 4 shows that the normal modes over a broad range of k/N, especially over an intermediate range from $k/N \simeq 0.1$ to 0.45, make nonnegligible contributions to the heat transport. This shows that the heat transport mechanism of the UFL is quite different from that of the FPUT lattice, which exhibits the nonballistic anomalous heat transport. In the FPUT lattice, only the normal modes with small k make a dominant contribution while J_H is strongly suppressed for the other larger k as N increases [31]. This suggests that those small k modes form solitons and they induce the anomalous heat transport in the FPUT lattice. In contrast, J_H is small for $k \simeq 0$, and this suggests that solitons are not formed and the normal modes, i.e., phonons, are the main heat carriers in the UFL. The heat transport by phonon is the situation supposed in Peierls's hypothesis.

To identify the thermal energy carriers precisely, we computed the space-time Fourier spectrum defined by

$$S(k, \omega) = \frac{1}{\sqrt{\tau}} \int_0^\tau u_k(t) e^{-i\omega t} dt, \tag{18}$$

where u_k is the mode amplitude defined by Eq. (15) and τ is a time interval taken sufficiently long. Figure 5 shows the magnitude of $|S(k, \omega)|^2$ by color. There clearly appears a narrow striplike curve indicated by bright red color, which represents large values, above the harmonic dispersion curve.

Equation (2) has the traveling wave solutions

$$q_n(t) = A \cos(kn - \omega t), \quad n \in \mathbb{Z}, \tag{19}$$

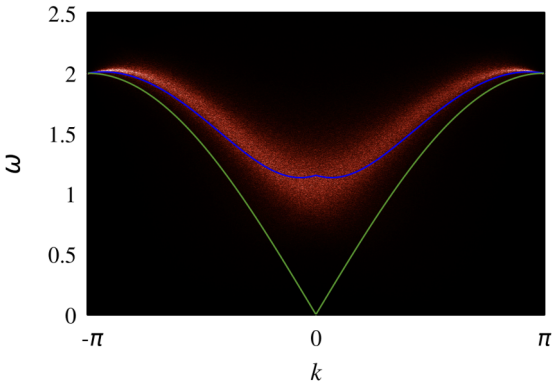

FIG. 5. Space-time Fourier spectrum of the steady heat transport state. $|S(k,\omega)|^2$ is presented by color. Parameters are $N = 4096$, $\mu_0 = 0$, $\mu_1 = 1$, and $\beta = 0.1$. Dispersion curve of the harmonic lattice ($\beta = 0$) and that of Eq. (20) are shown by green and blues lines, respectively.

where ω depends on (k, A), and it is given by the nonlinear dispersion relation

$$\omega = \sqrt{\nu_k^2 + (3/2)\,\pi(\pi - |k|)\,\beta A^2}, \tag{20}$$

where ν_k^2 is given by Eq. (5). We call this traveling wave the *nonlinear phonon*. The solution given by Eq. (19) is proved to be an exact one for $k \in [\pi/3, \pi]$ in a similar manner to the proof in Ref. [15], while it is an approximate one for $k \in [0, \pi/3)$.

The curve of Eq. (20) fitted to the numerical result by adjusting A is shown by blue line in Fig. 5, and it is in good agreement with the narrow striplike curve. A further numerical evidence is given in Appendix E. Based on this agreement, we may conclude that the thermal energy is carried by the nonlinear phonons. Moreover, Fig. 5 indicates that the nonlinear phonons propagate with subsonic velocities, since their maximal group velocity $\max_{k\in[0,\pi]} \partial\omega/\partial k$, which can be estimated from the curve of Eq. (20) in Fig. 5, is smaller than the sound velocity $\partial\nu_k/\partial k|_{k=+0}$. We note that each of the nonlinear phonons does not propagate independently, but they exchange their energy via the normal processes during propagation, because superpositions of Eq. (19) are no longer exact or approximate solutions of Eq. (2).

V. CONCLUSIONS

We constructed nonlinear lattices having a special type of long-range quartic interaction potential such that the umklapp process vanishes and only the normal processes exist, which we call the UFL. It is possible by using the UFL to directly verify Peierls's hypothesis that only the umklapp processes can cause the thermal resistance while the normal ones do not. Considering two types of the UFLs with and without the harmonic onsite potential, we studied their heat transport property by nonequilibrium molecular dynamics simulation. The numerical results and the experimental formula have shown that the ballistic heat transport, i.e., $\kappa \propto N$, occurs in the UFLs, and justify Peierls's hypothesis. Moreover, we pointed out the existence of the nonlinear phonons and showed that they are the thermal energy carriers which propagate with subsonic velocities. Finally, we emphasize that the UFL can be a good starting point to study the mechanism of emerging of the thermal resistance based on dynamics. It may be possible to clarify how the thermal resistance emerges via the umklapp processes by perturbing the UFL.

ACKNOWLEDGMENT

The authors were supported by a Grant-in-Aid for Scientific Research (C), 19K03654, from Japan Society for the Promotion of Science (JSPS).

APPENDIX A: PROOF OF NONCONSERVATION OF TOTAL MOMENTUM

We show nonconservation of the total momentum in Eq. (2). Precisely speaking, the total momentum $\sum_{n=-\infty}^{\infty} p_n$ of the infinite UFL does not necessarily have a finite value but may diverge. So, we employ its counterpart which is defined by a finite sum. Fix an arbitrary $N \in \mathbb{N}$, and impose the spatial periodicity condition $q_{n+N} = q_n$, $n \in \mathbb{Z}$ to Eq. (2). This is equivalent to considering a finite UFL consisting of N particles under the periodic boundary condition, instead of the infinite UFL.

Let $M_N = \sum_{n=1}^{N} p_n$. We prove nonconservation of M_N. It can be checked that Eq. (2) has a solution of the form $q_n(t) = \phi(t)$, $n \in \mathbb{Z}$, in which all the variables q_n have the same displacement ϕ. This solution apparently satisfies the spatial periodicity condition $q_{n+N} = q_n$. If we substitute this form into Eq. (2), then we have the equation

$$\ddot{\phi} = -\mu_0\phi - \sigma\phi^3, \tag{A1}$$

where $\sigma = 16\beta \sum_{m=1}^{\infty}(2m-1)^{-2}$. Equation (A1) is regarded as that of a Hamiltonian oscillator with the potential $V(\phi) = \mu_0\phi^2/2 + \sigma\phi^4/4$, which is a single-well potential due to $\mu_0 \geqslant 0$ and $\sigma > 0$. It is clear that this equation has a family of nonconstant periodic solutions. Choose an arbitrary solution from the family. Along this solution, $\dot{\phi}(t)$ is a nonconstant periodic function of t. This fact implies that $M_N = N\dot{\phi}(t)$ is not conserved. Thus, it has been proved that Eq. (2) does not conserve the total momentum in the sense that M_N is not conserved for any $N \in \mathbb{N}$.

APPENDIX B: DERIVATION OF EQUATION OF MOTION IN NORMAL MODE COORDINATES

We describe derivation of Eq. (4) in the main text via two steps. In the first step, we consider a class of lattices with general quartic nonlinear interaction potentials, and derive its equation of motion in normal mode coordinates. In the second step, we assume the case of UFL and derive Eq. (4).

1. Normal mode equation for general nonlinear lattices

Consider a class of infinite lattices described by the Hamiltonian

$$H_{\rm gen} = \sum_{n=-\infty}^{\infty} \frac{1}{2} p_n^2 + \sum_{n=-\infty}^{\infty} \left[\frac{\mu_0}{2} q_n^2 + \frac{\mu_1}{2}(q_{n+1} - q_n)^2 \right] + \frac{\beta}{4} \sum_{n=-\infty}^{\infty} \sum_{r=1}^{\infty} b_r (q_{n+r} - \varepsilon^r q_n)^4, \tag{B1}$$

where μ_0 and μ_1 are nonnegative constants, $\beta > 0$ is the nonlinearity strength, b_r is the coupling strength between the rth neighboring particles, and $\varepsilon \in \{-1, 1\}$. This is a slightly generalized version of Hamiltonian Eq. (1), and it describes general nonlinear lattices with quartic two-body interactions. For instance, Hamiltonian Eq. (B1) describes the UFL when $b_r = 1/r^2$ and $\varepsilon = -1$, while it describes the FPUT-β lattice when $b_r = \delta_{r,1}$, $\varepsilon = 1$, and $\mu_0 = 0$, where $\delta_{r,1}$ is Kronecker delta.

The equations of motion derived from the Hamiltonian Eq. (B1) are given by

$$\ddot{q}_n = -\mu_0 q_n + \mu_1(q_{n+1} - 2q_n + q_{n-1}) + \beta \sum_{r=1}^{\infty} b_r[(\varepsilon^r q_{n+r} - q_n)^3 - (q_n - \varepsilon^r q_{n-r})^3], \quad \text{(B2)}$$

where $n \in \mathbb{Z}$.

The normal mode coordinates $U(k)$ are defined by the discrete Fourier transformation as follows:

$$U(k) = \frac{1}{\sqrt{2\pi}} \sum_{n=-\infty}^{\infty} q_n e^{-ikn}, \quad k \in (-\pi, \pi], \quad \text{(B3)}$$

where k is restricted in the first Brillouin zone $\mathbb{T} = (-\pi, \pi]$. The inverse transformation is given by

$$q_n = \frac{1}{\sqrt{2\pi}} \int_{\mathbb{T}} U(k) e^{ikn} dk, \quad n \in \mathbb{Z}. \quad \text{(B4)}$$

Performing the discrete Fourier transformation to both sides of Eq. (B2), we have

$$\ddot{U}(k) + \nu_k^2 U(k) = \frac{\beta}{\sqrt{2\pi}} \sum_{n=-\infty}^{\infty} e^{-ikn} \times \sum_{r=1}^{\infty} b_r[(\varepsilon^r q_{n+r} - q_n)^3 - (q_n - \varepsilon^r q_{n-r})^3], \quad \text{(B5)}$$

where $\nu_k^2 = \mu_0 + 4\mu_1 \sin^2(k/2)$. Using Eq. (B4), we have

$$\varepsilon^r q_{n+r} - q_n = \varepsilon^r \sqrt{\frac{2}{\pi}} \int_{\mathbb{T}} U(k) e^{ikn} e^{irk/2} g_r(k) dk, \quad \text{(B6)}$$

$$q_n - \varepsilon^r q_{n-r} = \sqrt{\frac{2}{\pi}} \int_{\mathbb{T}} U(k) e^{ikn} e^{-irk/2} g_r(k) dk, \quad \text{(B7)}$$

where $g_r(k)$ is given by

$$g_r(k) = \frac{1}{2}(e^{irk/2} - \varepsilon^r e^{-irk/2}). \quad \text{(B8)}$$

Substituting Eqs. (B6) and (B7) into the right-hand side of Eq. (B5), we have

$$\begin{aligned}
\ddot{U}(k) + \nu_k^2 U(k) &= \frac{\beta}{\sqrt{2\pi}} \sum_{n=-\infty}^{\infty} e^{-ikn} \sum_{r=1}^{\infty} b_r \left[\prod_{j=1}^{3} \left\{ \varepsilon^r \sqrt{\frac{2}{\pi}} \int_{\mathbb{T}} U(k_j) e^{ik_j n} e^{irk_j/2} g_r(k_j) dk_j \right\} \right. \\
&\quad \left. - \prod_{j=1}^{3} \left\{ \sqrt{\frac{2}{\pi}} \int_{\mathbb{T}} U(k_j) e^{ik_j n} e^{-irk_j/2} g_r(k_j) dk_j \right\} \right] \\
&= \frac{2\beta}{\pi^2} \sum_{n=-\infty}^{\infty} \sum_{r=1}^{\infty} b_r \int_{\mathbb{T}^3} dk_1 dk_2 dk_3 U(k_1) U(k_2) U(k_3) \{\varepsilon^r e^{i(k_1+k_2+k_3-k)r/2} e^{irk/2} - e^{-i(k_1+k_2+k_3-k)r/2} e^{-irk/2}\} \\
&\quad \times G_r(k_1, k_2, k_3)\, e^{i(k_1+k_2+k_3-k)n}, \quad \text{(B9)}
\end{aligned}$$

where G_r is defined by

$$G_r(k_1, k_2, k_3) = g_r(k_1) g_r(k_2) g_r(k_3). \quad \text{(B10)}$$

As for the sum over n in Eq. (B9), recall the formula

$$\sum_{n=-\infty}^{\infty} e^{incx} = \frac{2\pi}{c} \sum_{m=-\infty}^{\infty} \delta(x - 2\pi m/c), \quad \text{(B11)}$$

where $c,\ x \in \mathbb{R}$ are constants. We can calculate the sum over n in Eq. (B9) by applying Eq. (B11) with $c = 1$ and $x = k_1 + k_2 + k_3 - k$. Then, we obtain

$$\sum_{n=-\infty}^{\infty} e^{i(k_1+k_2+k_3-k)n} = 2\pi \sum_{m=-\infty}^{\infty} \delta(k_1 + k_2 + k_3 - k - 2\pi m). \quad \text{(B12)}$$

Using this and denoting $\lambda = k_1 + k_2 + k_3 - k$, we can rewrite Eq. (B9) as follows:

$$\ddot{U}(k) + \nu_k^2 U(k) = \frac{4\beta}{\pi} \sum_{r=1}^{\infty} b_r \int_{\mathbb{T}^3} dk_1 dk_2 dk_3 U(k_1) U(k_2) U(k_3) \{\varepsilon^r e^{i(\lambda+k)r/2} - e^{-i(\lambda+k)r/2}\} G_r(k_1, k_2, k_3) \sum_{m=-\infty}^{\infty} \delta(\lambda - 2\pi m). \quad \text{(B13)}$$

Since $-\pi < k_j \leqslant \pi$ and $-\pi \leqslant -k < \pi$, we have $-4\pi < \lambda < 4\pi$. Thus, there are only three possible values of λ, i.e., $\lambda = 0, \pm 2\pi$, which correspond to $m = 0, \pm 1$, respectively. Taking into account this fact, we can rewrite Eq. (B13) as

$$\ddot{U}(k) + \nu_k^2 U(k) = \frac{4\beta}{\pi} \int_{\mathbb{T}^3} dk_1 dk_2 dk_3 U(k_1) U(k_2) U(k_3) \sum_{m=-1}^{1} \delta(\lambda - 2\pi m) \phi_m(k_1, k_2, k_3, k), \tag{B14}$$

where ϕ_m is defined by

$$\phi_m(k_1, k_2, k_3, k) = \sum_{r=1}^{\infty} b_r \{\varepsilon^r e^{i\pi mr} e^{irk/2} - e^{-i\pi mr} e^{-irk/2}\} G_r(k_1, k_2, k_3). \tag{B15}$$

2. Normal mode equation for UFL

Hereafter, we assume the case of UFL, i.e., $b_r = 1/r^2$ and $\varepsilon = -1$, and derive Eq. (4). If we use $e^{i\pi mr} = e^{-i\pi mr}$, which follows from $m = 0, \pm 1$, and denote $k' = -k$, then we have

$$\phi_m(k_1, k_2, k_3, -k') = \sum_{r=1}^{\infty} \frac{1}{r^2} \{(-1)^r e^{-ik'r/2} - e^{ik'r/2}\} e^{i\pi mr} G_r(k_1, k_2, k_3). \tag{B16}$$

Let $a = k_1/2$, $b = k_2/2$, $c = k_3/2$, and $d = k'/2$. If we divide the sum in Eq. (B16) into two parts and use Eqs. (B8) and (B10), then we obtain

$$\phi_m(k_1, k_2, k_3, -k') = K_o(m) + K_e(m), \tag{B17}$$

where $K_o(m)$ and $K_e(m)$ are given by

$$K_o(m) = -2 \sum_{r=\text{odd}} \frac{(-1)^m}{r^2} \cos(ra) \cos(rb) \cos(rc) \cos(rd), \tag{B18}$$

$$K_e(m) = -2 \sum_{r=\text{even}} \frac{1}{r^2} \sin(ra) \sin(rb) \sin(rc) \sin(rd). \tag{B19}$$

The sums in Eqs. (B18) and (B19) are taken over all odd and even $r \in \mathbb{N}$, respectively.

We want to show $\phi_m(k_1, k_2, k_3, -k') = 0$ under the condition $k_1 + k_2 + k_3 + k' = 2\pi m$ for $m = \pm 1$. It is easy to see that ϕ_m has the property

$$\phi_m(k_1, k_2, k_3, -k') = \phi_{-m}(-k_1, -k_2, -k_3, k'). \tag{B20}$$

Because of this property, if $\phi_m(k_1, k_2, k_3, -k') = 0$ holds for any (k_1, k_2, k_3, k') satisfying $k_1 + k_2 + k_3 + k' = 2\pi m$, then $\phi_{-m}(k_1, k_2, k_3, -k') = 0$ also holds for any (k_1, k_2, k_3, k') satisfying $k_1 + k_2 + k_3 + k' = -2\pi m$. Thus, it is enough to consider one of the $m = \pm 1$ cases. In what follows, we show $\phi_1(k_1, k_2, k_3, -k') = 0$.

A simple calculation using Eqs. (B18) and (B19) leads to

$$\begin{aligned} K_o(m) = -\frac{1}{4} \sum_{r=\text{odd}} \frac{(-1)^m}{r^2} \{&\cos(r(a+b+c+d)) + \cos(r(a-b+c+d)) + \cos(r(a+b-c+d)) + \cos(r(a+b+c-d)) \\ &+ \cos(r(a+b-c-d)) + \cos(r(a-b+c-d)) + \cos(r(a-b-c+d)) + \cos(r(a-b-c-d))\}, \end{aligned} \tag{B21}$$

$$\begin{aligned} K_e(m) = -\frac{1}{4} \sum_{r=\text{even}} \frac{1}{r^2} \{&\cos(r(a+b+c+d)) - \cos(r(a-b+c+d)) - \cos(r(a+b-c+d)) - \cos(r(a+b+c-d)) \\ &+ \cos(r(a+b-c-d)) + \cos(r(a-b+c-d)) + \cos(r(a-b-c+d)) - \cos(r(a-b-c-d))\}. \end{aligned} \tag{B22}$$

Assuming $m = 1$ and substituting Eqs. (B21) and (B22) into Eq. (B17), we obtain

$$\begin{aligned} \phi_1(k_1, k_2, k_3, -k') = &\frac{1}{4} \sum_{r=1}^{\infty} \frac{(-1)^{r-1}}{r^2} \{\cos(r(a+b+c+d)) + \cos(r(a+b-c-d)) \\ &+ \cos(r(a-b+c-d)) + \cos(r(a-b-c+d))\} \\ &+ \frac{1}{4} \sum_{r=1}^{\infty} \frac{1}{r^2} \{\cos(r(a-b-c-d)) + \cos(r(a-b+c+d)) \\ &+ \cos(r(a+b-c+d)) + \cos(r(a+b+c-d))\}. \end{aligned} \tag{B23}$$

Recall that $a, b, c \in (-\pi/2, \pi/2]$ and $d \in [-\pi/2, \pi/2)$, which follow from their definitions. We show $\phi_1 = 0$ for the wider range $a, b, c, d \in [-\pi/2, \pi/2]$. Since ϕ_1 is invariant for any permutation of a, b, c, d, we can assume $\pi/2 \geqslant a \geqslant b \geqslant c \geqslant d \geqslant -\pi/2$. Recall that $a+b+c+d = \pi$ holds when $m = 1$. Note that (i) $a, b > 0$ and (ii) $c \geqslant 0$ have to hold, because if $b \leqslant 0$, then $a \geqslant a+b+c+d = \pi$ and this contradict with $\pi/2 \geqslant a$, and if $c < 0$, then $a+b > a+b+c+d = \pi$ and this contradict with $\pi \geqslant a+b$. In addition, note that the sum of any pair taken from $\{a, b, c, d\}$ is nonnegative, i.e., (iii) $x+y \geqslant 0$ for $x, y \in \{a, b, c, d\}$ such that $x \neq y$, because if $x+y < 0$, then $z+w > x+y+z+w = a+b+c+d = \pi$ being in contradiction with $\pi \geqslant z+w$, where w and z are the elements other than x and y.

Noting the properties (i)–(iii), we can evaluate the ranges of arguments of cosine functions in Eq. (B23) as follows:

In the first sum,

$$a+b+c+d = \pi,$$
$$0 \leqslant a+b-c-d = a+b-(c+d) \leqslant a+b \leqslant \pi \quad (\because a \geqslant c, b \geqslant d; c+d \geqslant 0),$$
$$0 \leqslant a-b+c-d = a+c-(b+d) \leqslant a+c \leqslant \pi \quad (\because a \geqslant b, c \geqslant d; b+d \geqslant 0),$$
$$-\pi \leqslant -(b+c) \leqslant a-b-c+d \leqslant a+d \leqslant \pi \quad (\because a+d \geqslant 0; b+c \geqslant 0);$$

in the second sum,

$$0 \leqslant -(a-b-c-d) = b+c+d-a = \pi - 2a \leqslant \pi \quad (\because 0 \leqslant 2a \leqslant \pi),$$
$$0 \leqslant a-b+c+d = a+c+d-b = \pi - 2b \leqslant \pi \quad (\because 0 \leqslant 2b \leqslant \pi),$$
$$0 \leqslant a+b-c+d = a+b+d-c = \pi - 2c \leqslant \pi \quad (\because 0 \leqslant 2c \leqslant \pi),$$
$$0 \leqslant a+b+c-d = \pi - 2d \leqslant \pi + 2|d| \leqslant 2\pi \quad (\because -\pi \leqslant 2d \leqslant \pi).$$

To compute the two sums in Eq. (B23), recall the following formula:

$$\sum_{r=1}^{\infty} \frac{\cos rx}{r^2} = \frac{1}{4}(\varphi(x) - \pi)^2 - \frac{\pi^2}{12}, \tag{B24}$$

where $\varphi(x)$ is the function given by

$$\varphi(x) = x - 2\pi l \quad \text{for } x \in (2\pi l, 2\pi(l+1)], \ l \in \mathbb{Z}. \tag{B25}$$

If we replace x with $x+\pi$ in Eq. (B24), then we can modify the above formula as follows:

$$\sum_{r=1}^{\infty} \frac{(-1)^{r-1}}{r^2} \cos rx = \frac{\pi^2}{12} - \frac{x^2}{4}, \quad x \in [-\pi, \pi]. \tag{B26}$$

If we apply Eqs. (B24) and (B26) to Eq. (B23) with noting the ranges of arguments of cosine functions, which were shown above, then we have

$$\begin{aligned}
&\phi_1(k_1, k_2, k_3, -k') \\
&= \frac{1}{4} \cdot \left[\frac{\pi^2}{12} - \frac{\pi^2}{4} + \frac{\pi^2}{12} - \frac{(a+b-c-d)^2}{4} \right. \\
&\quad + \frac{\pi^2}{12} - \frac{(a-b+c-d)^2}{4} + \frac{\pi^2}{12} - \frac{(a-b-c+d)^2}{4} \\
&\quad + \frac{\{(b+c+d-a)-\pi\}^2}{4} - \frac{\pi^2}{12} \\
&\quad + \frac{\{(a-b+c+d)-\pi\}^2}{4} - \frac{\pi^2}{12} \\
&\quad + \frac{\{(a+b-c+d)-\pi\}^2}{4} - \frac{\pi^2}{12} \\
&\quad \left. + \frac{\{(a+b+c-d)-\pi\}^2}{4} - \frac{\pi^2}{12} \right] \\
&= \frac{1}{16}(a+b+c+d)^2 - \frac{\pi}{4}(a+b+c+d) + \frac{3}{16}\pi^2 \\
&= 0,
\end{aligned} \tag{B27}$$

where we used $a+b+c+d = \pi$. Since it has been proved that $\phi_{\pm 1}(k_1, k_2, k_3, -k') = 0$ when $k_1+k_2+k_3+k' = \pm 2\pi$, Eq. (B14) reduces to

$$\begin{aligned}
\ddot{U}(k) + \nu_k^2 U(k) = \frac{4\beta}{\pi} \int_{\mathbb{T}^3} dk_1 dk_2 dk_3 \phi_0(k_1, k_2, k_3, k) \\
\times U(k_1) U(k_2) U(k_3) \delta(k_1 + k_2 + k_3 - k).
\end{aligned} \tag{B28}$$

This equals to Eq. (4).

APPENDIX C: RELATION BETWEEN UFL AND PISL

The PISL was originally constructed as a finite-size lattice with the periodic boundary condition [8,9]. Its extension to the infinite-size one is described by the Hamiltonian

$$\begin{aligned}
H = &\sum_{n=-\infty}^{\infty} \frac{1}{2} p_n^2 + \sum_{n=-\infty}^{\infty} \left[\frac{\mu_0}{2} q_n^2 + \frac{\mu_1}{2} (q_{n+1} - q_n)^2 \right] \\
&+ \beta \sum_{n=-\infty}^{\infty} \sum_{r=1}^{\infty} \frac{1}{4r^2} (q_{n+r} - q_n)^4,
\end{aligned} \tag{C1}$$

which corresponds to the case of $b_r = 1/r^2$ and $\varepsilon = 1$ in Eq. (B1). The equations of motion are given by

$$\begin{aligned}
\ddot{q}_n = &-\mu_0 q_n + \mu_1 (q_{n+1} - 2q_n + q_{n-1}) \\
&+ \beta \sum_{r=1}^{\infty} \frac{1}{r^2} [(q_{n+r} - q_n)^3 - (q_n - q_{n-r})^3],
\end{aligned} \tag{C2}$$

where $n \in \mathbb{Z}$. If we fix an arbitrary even $N \in \mathbb{N}$ and impose the periodicity condition $q_{n+mN} = q_n$, $m \in \mathbb{Z}$ in Eq. (C2), then it reduces to the equations of motion of the finite-size periodic PISL in Refs. [8,9].

Equations (1) and (C1) show that nonlinear potentials of the UFL and the PISL are transformed to each other by the staggered transformation $q_n \to (-1)^n q_n$. In this sense, these

two lattices correspond to each other. This correspondence implies that the two lattices have essentially the same dynamics when $\mu_0 = \mu_1 = 0$, i.e., the homogeneous potential case.

Let us define $\tilde{U}(m)$ via the transformation

$$\tilde{U}(m) = \frac{1}{\sqrt{2\pi}} \sum_{n=-\infty}^{\infty} (-1)^n q_n e^{-imn}, \quad m \in (-\pi, \pi], \tag{C3}$$

which is a composition of the staggered transformation and the discrete Fourier transformation defined by Eq. (B3). If we perform the above transformation to rewrite Eq. (C2) in terms of $\tilde{U}(m)$, then its nonlinear force part can be computed in the same manner as in the UFL. Noting the linear force part, we obtain the equation

$$\begin{aligned} &\ddot{\tilde{U}}(m) + \tilde{\nu}_m^2 \tilde{U}(m) \\ &= \frac{4\beta}{\pi} \int_{\mathbb{T}^3} dm_1 dm_2 dm_3 \phi_0(m_1, m_2, m_3, m) \\ &\quad \times \tilde{U}(m_1)\tilde{U}(m_2)\tilde{U}(m_3)\delta(m_1 + m_2 + m_3 - m), \end{aligned} \tag{C4}$$

where ϕ_0 is a time-independent function of (m_1, m_2, m_3, m) and $\tilde{\nu}_m^2$ is given by

$$\tilde{\nu}_m^2 = \mu_0 + 4\mu_1 \cos^2(m/2). \tag{C5}$$

Equation (C4) has the same form as Eq. (4), but note that the dependence of $\tilde{\nu}_m^2$ on m is different form that of ν_k^2 on k. In the nonhomogeneous potential case, the UFL and the PISL have different dynamics.

Equation (C4) shows that four normal modes are coupled only when their wave numbers satisfy the condition $m_1 + m_2 + m_3 - m = 0$ while the couplings of $\pm 2\pi$ are not allowed. This mode coupling rule is a peculiarity of the PISL, which is similar to that of the UFL.

APPENDIX D: DERIVATION OF THE SPECTRAL ENERGY FLUX FORMULA

Consider the total harmonic heat flux $J_{H,\mathrm{tot}}$ given by Eq. (14). We approximate $J_{H,\mathrm{tot}}$ as follows:

$$J_{H,\mathrm{tot}} \simeq -\frac{\mu_1}{2} \sum_{n=n_0+1}^{n_0+N} (\dot{q}_{n+1} + \dot{q}_n)(q_{n+1} - q_n), \tag{D1}$$

where $q_{n_0+N+1} = q_{n_0+1}$. The sum is taken only up to $n = n_0 + N - 1$ in the definition of $J_{H,\mathrm{tot}}$. In this approximation, we added the last term $-\mu_1(\dot{q}_{n_0+1} + \dot{q}_{n_0+N})(q_{n_0+1} - q_{n_0+N})/2$. Since we assume large values of N in our simulation, this last term is much smaller than the sum of other terms in Eq. (D1), and we can expect Eq. (D1) to be a good approximation.

If we substitute Eq. (15) into Eq. (D1), then we obtain

$$\begin{aligned} &J_{H,\mathrm{tot}} \\ &= -\frac{\mu_1}{2N} \sum_{n=1}^{N} \left\{ \sum_{m=-N/2+1}^{N/2} \dot{u}_m \left(e^{-i\theta m} + 1\right) e^{-i\theta mn} \right\} \\ &\quad \times \left\{ \sum_{k=-N/2+1}^{N/2} u_k (e^{-i\theta k} - 1) e^{-i\theta kn} \right\} \\ &= -\frac{\mu_1}{2N} \sum_{k,m=-N/2+1}^{N/2} \\ &\quad \times \left[\sum_{n=1}^{N} \dot{u}_m u_k (e^{-i\theta m} + 1)(e^{-i\theta k} - 1) e^{-i\theta(k+m)n} \right], \end{aligned}$$

where $\theta = 2\pi/N$. Calculating the sum with respect to n, we have

$$\begin{aligned} J_{H,\mathrm{tot}} = -\frac{\mu_1}{2N} &\sum_{k,m=-N/2+1}^{N/2} [\dot{u}_m u_k (e^{-i\theta m} + 1)(e^{-i\theta k} - 1) \\ &\times N(\delta_{k+m,0} + \delta_{k+m,N})], \end{aligned} \tag{D2}$$

where $\delta_{k+m,0}$ and $\delta_{k+m,N}$ are Kronecker delta. The condition $k + m = N$ holds only for $k = m = N/2$, and we have $e^{-i\theta m} + 1 = 0$ in this case. If we calculate the sum with respect to m in Eq. (D2), taking account of this fact, then we have

$$\begin{aligned} J_{H,\mathrm{tot}} &= -\frac{\mu_1}{2} \sum_{k=-N/2+1}^{N/2-1} u_k \dot{u}_{-k} (e^{i\theta k} + 1)(e^{-i\theta k} - 1) \\ &= i\mu_1 \sum_{k=-N/2+1}^{N/2-1} u_k \dot{u}_{-k} \cdot 2 \sin\frac{\pi k}{N} \cos\frac{\pi k}{N} \\ &= i \sum_{k=-N/2+1}^{N/2-1} \omega_k v_k u_k \dot{u}_{-k}, \end{aligned} \tag{D3}$$

where $\omega_k = 2\sqrt{\mu_1}\,|\sin(\pi k/N)|$ and $v_k = \sqrt{\mu_1}\mathrm{sgn}(k)\cos(\pi k/N)$. Note that the term for $k = 0$ vanishes due to $\omega_0 = 0$. Dividing the sum in Eq. (D3) into two parts, we can rewrite $J_{H,\mathrm{tot}}$ as follows:

$$\begin{aligned} J_{H,\mathrm{tot}} &= i \sum_{k=1}^{N/2-1} \omega_k v_k u_k \dot{u}_{-k} + i \sum_{k=1}^{N/2-1} \omega_{-k} v_{-k} u_{-k} \dot{u}_k \\ &= \frac{1}{i} \sum_{k=1}^{N/2-1} \omega_k v_k (\dot{u}_k u_{-k} - u_k \dot{u}_{-k}) \\ &= \sum_{k=1}^{N/2-1} 2\,\omega_k v_k\,\mathrm{Im}[\dot{u}_k \bar{u}_k] \\ &= \sum_{k=1}^{N/2-1} J_H(k), \end{aligned} \tag{D4}$$

where we used $\omega_{-k} v_{-k} = -\omega_k v_k$ and $u_{-k} = \bar{u}_k$.

APPENDIX E: NUMERICAL EVIDENCE FOR NONLINEAR PHONONS

In Fig. 5, the curve of $|S(k, \omega)|^2$ is not a sharp line but exhibits nonsmall line width. In addition, there is slight discrepancy between the dispersion curve of Eq. (20) and the average profile of $|S(k, \omega)|^2$ curve, i.e., the middle line of its striplike curve. Due to these facts, it might not be a fully convincing scenario that the nonlinear phonons emerge and carry the thermal energy in steady heat transport state. In this section, we give an additional numerical evidence to ensure this scenario.

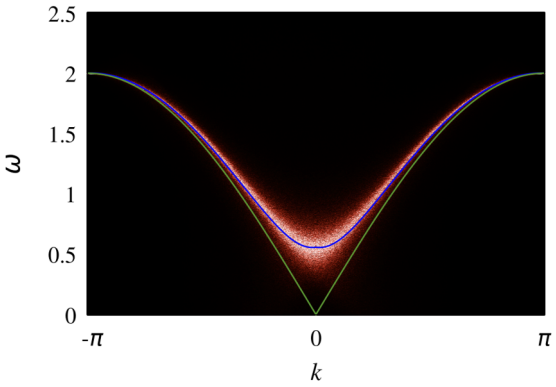

FIG. 6. Space-time Fourier spectrum of the steady heat transporting state in the UFL of weak nonlinearity $\beta = 0.01$. $|S(k,\omega)|^2$ is presented by color. Parameters are $N = 4096$, $\mu_0 = 0$, and $\mu_1 = 1$. Dispersion curve of the harmonic lattice ($\beta = 0$) and that of Eq. (20) are shown by green and blues lines, respectively.

We have assumed that the amplitude A of nonlinear phonons is a constant independent of k when fitting Eq. (20) to the numerical result of $|S(k,\omega)|^2$. However, in actual, it may be expected that the value of A fluctuates in time and moreover the temporal average of A depends on k, provided that the nonlinear phonons emerge. If we take into account these points, then we may write the amplitude A in the form

$$A = A_0 + \delta A(k) + \varepsilon(k,t), \tag{E1}$$

where A_0 is a constant, $A_0 + \delta A(k)$ represents the temporal average of A for k, and $\varepsilon(k,t)$ represents the temporal fluctuation in A for a given k. This form may explain differences between the numerical result of $|S(k,\omega)|^2$ and the dispersion curve of Eq. (20): $\varepsilon(k,t)$ causes the line width and $\delta A(k)$ causes a deviation of the average profile from Eq. (20) under substitution of Eq. (E1) into Eq. (20).

The A-dependent term is in proportion to β in Eq. (20). This fact suggests that the influences of $\delta A(k)$ and $\varepsilon(k,t)$ are small for small values of β, resulting in a better agreement of $|S(k,\omega)|^2$ with Eq. (20) for a k-independent constant A. Figure 6 shows $|S(k,\omega)|^2$ computed for the UFL of weak nonlinearity $\beta = 0.01$, where the other parameters are the same as in Fig. 5. An excellent agreement is clearly observed. This agreement validates the above-mentioned scenario.

[1] C. W. Chang, D. Okawa, H. Garcia, A. Majumdar, and A. Zettl, Phys. Rev. Lett. **101**, 075903 (2008).
[2] C. Kittel, *Introduction to Solid State Physics* (Wiley, New York, NY, 2004).
[3] N. Ashcroft and N. Mermin, *Solid State Physics* (Saunders College Publishing, New York, 1976).
[4] R. E. Peierls, *Quantum Theory of Solids* (Oxford University Press, London, 1955).
[5] R. E. Peierls, On the kinetic theory of thermal conduction in crystals, in *Selected Scientific Papers of Sir Rudolf Peierls*, edited by R. H. Dalitz and R. Peierls (World Scientific, Singapore, 1997).
[6] E. A. Jackson, Rocky Mount. J. Math. **8**, 127 (1978).
[7] S. Lepri, R. Livi, and A. Politi, Phys. Rep. **377**, 1 (2003).
[8] Y. Doi and K. Yoshimura, Phys. Rev. Lett. **117**, 014101 (2016).
[9] Y. Doi and K. Yoshimura, Nonlinearity **33**, 5142 (2020).
[10] A. J. Sievers and S. Takeno, Phys. Rev. Lett. **61**, 970 (1988).
[11] J. B. Page, Phys. Rev. B **41**, 7835 (1990).
[12] K. Yoshimura and Y. Doi, J. Diff. Eq. **298**, 560 (2021).
[13] K. Yoshimura, Y. Doi, and M. Kimura, Localized modes in nonlinear discrete systems, in *Progress in Nanophotonics III*, edited by M. Ohtsu and T. Yatsui (Springer, New York, 2014), p. 119.
[14] D. Bagchi, Phys. Rev. E **95**, 032102 (2017).
[15] K. Yoshimura and Y. Doi, in *Proceedings of the 2019 International Symposium on Nonlinear Theory and Its Applications* (IEICE, Tokyo, 2019), p. 399.
[16] K. Yoshimura, Y. Doi, and M. Ebisu, in *Proceedings of the 2020 International Symposium on Nonlinear Theory and Its Applications* (IEICE, Tokyo, 2020), p. 181.
[17] D. Bagchi, Phys. Rev. E **104**, 054108 (2021).
[18] J. Wang, S. V. Dmitriev, and D. Xiong, Phys. Rev. Res. **2**, 013179 (2020).
[19] S. Iubini, P. Di Cintio, S. Lepri, R. Livi, and L. Casetti, Phys. Rev. E **97**, 032102 (2018).
[20] G. Casati, J. Ford, F. Vivaldi, and W. M. Visscher, Phys. Rev. Lett. **52**, 1861 (1984).
[21] D. J. R. Mimnagh and L. E. Ballentine, Phys. Rev. E **56**, 5332 (1997).
[22] T. Prosen and M. Robnik, J. Phys. A **25**, 3449 (1992).
[23] B. Hu, B. Li, and H. Zhao, Phys. Rev. E **57**, 2992 (1998).
[24] B. Hu, B. Li, and H. Zhao, Phys. Rev. E **61**, 3828 (2000).
[25] K. Aoki and D. Kusnezov, Phys. Lett. A **265**, 250 (2000).
[26] P. D. Cintio, S. Iubini, S. Lepri, and R. Livi, Chaos, Solitons Fractals **117**, 249 (2018).
[27] C. Giardiná, R. Livi, A. Politi, and M. Vassalli, Phys. Rev. Lett. **84**, 2144 (2000).
[28] G. R. Lee-Dadswell, E. Turner, J. Ettinger, and M. Moy, Phys. Rev. E **82**, 061118 (2010).
[29] S. Lepri, Eur. Phys. J. B **18**, 441 (2000).
[30] S. Lepri, R. Livi, and A. Politi, Physica D **119**, 140 (1998).
[31] G. Dematteis, L. Rondoni, D. Proment, F. De Vita, and M. Onorato, Phys. Rev. Lett. **125**, 024101 (2020).
[32] T. Hatano, Phys. Rev. E **59**, R1 (1999).
[33] M. Toda, Phys. Scr. **20**, 424 (1979).
[34] T. Prosen and D. K. Campbell, Chaos **15**, 015117 (2005).
[35] C. Giardinà and J. Kurchan, J. Stat. Mech. (2005) P05009.